2014

Performance And Results For Quartz Detector For The Superhms Spectrometer At Hall C Jefferson Lab

Jr. Benjamin Griego

North Carolina Agricultural and Technical State University

Performance and Results for Quartz Detector for the SuperHMS Spectrometer at Hall_C Jefferson Lab

Benjamin F Griego Jr.

North Carolina A&T State University

A thesis submitted to the graduate faculty

in partial fulfillment of the requirements for the degree of

MASTER OF SCIENCE

Department: Physics

Major: Physics

Major Professor: Dr. A. Ahmidouch

Greensboro, North Carolina

2014

The Graduate School

North Carolina Agricultural and Technical State University

This is to certify that the Masters Thesis of

Benjamin F Griego Jr.

has met the thesis requirements of

North Carolina Agricultural and Technical State University

Greensboro, North Carolina

2014

Approved by:

Dr. A. Ahmidouch Major Professor	Dr. S. Danagoulian Committee Member
Dr. K.M. Flurchick Committee Member	Dr. A. Ahmidouch Department Chairperson
Dr. Sanjiv Sarin Dean, The Graduate School	

DEDICATION

To all those that have had to do whatever it takes to pursue your positive passion.

BIOGRAPHICAL SKETCH

Benjamin Francisco Griego Jr. was born in Albuquerque, New Mexico. He graduated high school in Olympia, Washington and eventually moved to Fort Collins, Colorado to begin his college career at Front Range Community College. After obtaining his A.S., he transferred to Colorado State University (CSU) where he received a B.S. in Physics with a minor in Mathematics. While at CSU, he began research on variable stars which lead him to the pursue an advanced degree at North Carolina Agricultural and Technical State University (NCAT). He was awarded the Graduate Student Merit Award for 2013–2014. He is a candidate for the Master of Science degree in Physics.

ACKNOWLEDGEMENTS

I would like to thank all those that have helped me on the interesting journey. First and foremost, my wife Juliette. It has been a very long time coming but at least now there is light in the tunnel. The list of those who have helped me is too long to include here, but if you know me and are reading this, then you were one who helped me. To my family, thank you for the words of wisdom and support throughout everything in my journey. There is no way I could be where I am without the help and encouragement of those professors and faculty who believed in me and guided me throughout my academic career.

TABLE OF CONTENTS

LIST OF TABLES

Table **Page**

LIST OF FIGURES

Figure **Page**

ABSTRACT

A quartz detector has been constructed to be part of the trigger system for the Super High Momentum Spectrometer (SHMS). The SHMS will play a pivotal role in carrying out the 12-GeV physics program at Hall-C Jefferson Lab. The quartz hodoscope consists of twenty one fused silica bars. Each bar is 125 cm long, 5.5 cm wide, 2.5 cm thick, and is viewed by a UV-sensitive PMT on each end. The quartz hodoscope's task is to provide a clean detection of charged particles, a high level of background suppression, and an accurate tracking efficiency determination. Initial test results of the quartz detectors which include light yield and position resolution will be presented.

CHAPTER 1

Introduction

Detecting particles is an essential component of modern-day nuclear and particle physics. Designing and constructing the apparatus which ultimately detects the particles must be taken with the utmost concern. The focus of this project is the development, construction, and testing of the 21 quartz bar Hodoscope to be part of the trigger system for the Super High Momentum Spectormeter (SHMS) detector at Hall C Jefferson Lab (JLab).

The SHMS is the main detector upgrade component for the 12 GeV upgrade at JLab Hall C. The 12 GeV physics program will make use of the newly constructed SHMS and will work in conjunction with the existing High Momentum Spectormeter (HMS). The quartz hodoscope task is to provide a clean detection of charged particles with a 99.9% efficiency, a high level of background suppression, and an accurate tracking efficiency determination. The SHMS momentum range is 2.5 to 11 GeV/c with an acceptance of -15% to +25% at a resolution of $< 0.2\%$. The horizontal and vertical angle acceptance will be ± 18 mrad and ± 50 mrad respectively and a solid angle acceptance of 3.8 msr. The horizontal bend angle is 3° and the vertical bend angle is 18.5°.

This project is focusing on the quartz detector package for the SHMS assembled by NCAT. A description of the stages of assembly of the detectors, their testing and calibration, and initial results of testing will be presented.

CHAPTER 2

Future 12-GeV Physics at Hall C JLab

The 12-GeV upgrade will provide scientists at JLab the necessary tools to investigate the energy regime of quantum chromo-dynamics (QCD), perturbative QCD, associated quark model along with other atomic and subatomic theories and measurements. Examples of planned and approved experiments include the Measurement of the Charged Pion Form Factor to High Q^2 and the Measurement of Neutron Spin Asymmetry A_1^n in the Valence Quark Region Using an 11 GeV Beam and a Polarized ^{3}He Target in Hall C.

Table 2.1 is summary of some of the experiments approved to run in Hall–C with 12-GeV beam [1]. The scope of these experiments ranges from nucleon electromagnetic structure, nucleon spin structure, color transparency, meson spectroscopy nucleon and pion form factors. In all these experiments, the SHMS will play a pivotal role.

Table 2.1: Sample of experiments approved for SHMS

Experiment	Title	Rating
E12-06-101	Measurement of the Charged Pion Form Factor to High Q^2	A
E12-06-110	Measurement of Neutron Spin Asymmetry A_1^n in the Valence Quark Region Using an 11 GeV Beam and a Polarized ^3He Target in Hall C	A
E12-06-121	A Path to 'Color Polarizabilities' in the Neutron: A Precision Measurement of the Neutron g_2 and d_2 at High Q^2 in Hall C	A–
E12-10-008	Detailed studies of the nuclear dependence of F_2 in light nuclei.	A–
E12-07-105	Scaling Study of the L-T Separated Pion Electroproduction Cross Section at 11 GeV	A–
E12-09-002	Precise Measurement of π^+/π^- Ratios in Semi-inclusive Deep Inelastic Scattering Part I: Charge Symmetry violating Quark Distributions	A-
E12-09-017	Transverse Momentum Dependence of Semi-Inclusive Pion Production	A–
E12-13-007	Measurement of Semi-Inclusive π^0 Production as Validation of Factorization	A–
E12-13-010	Exclusive Deeply Virtual Compton and Neutral Pion Cross-Section Measurements in Hall C	A

CHAPTER 3

Super High Momentum Spectrometer

The major upgrade to Hall C's detector system is the addition of the SHMS. The SHMS, like the HMS, is a QQQD spectrometer, see Figure 3.1, but will allow the measurment of higher momenta than the HMS.

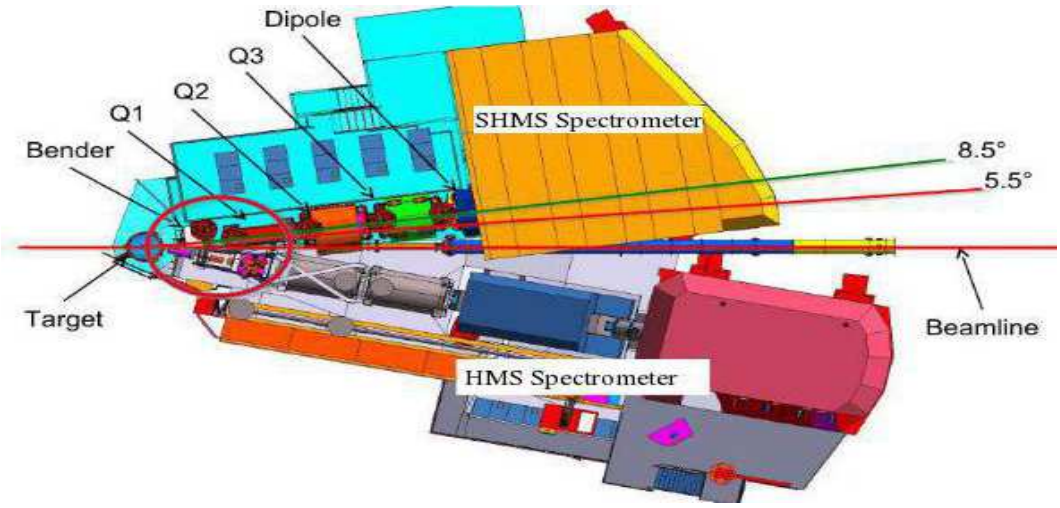

Figure 3.1: Full view of Hall C detector setup

All the detectors are housed within the large shield house which is designed to minimize background radiation. The detector package will consist of a Cherenkov counter, a wire chamber tracking system, a scintillator triggering system S1X and S1Y, a heavy gas Cherenkov counter, S2X scintillator and S2Y hodoscope trigger system, and a calorimeter, see Figure 3.2.

One main difference between the SHMS and the currently installed HMS is the replacement of the fourth scintillator plane with the quartz hodoscope, S2Y. The quartz detectors will provide a clean detection of charged particles via Cherenkov radiation process. The production of the Cherenkov radiation can lead to the elimination of most of the background radiation by excluding all low energy particles with velocities

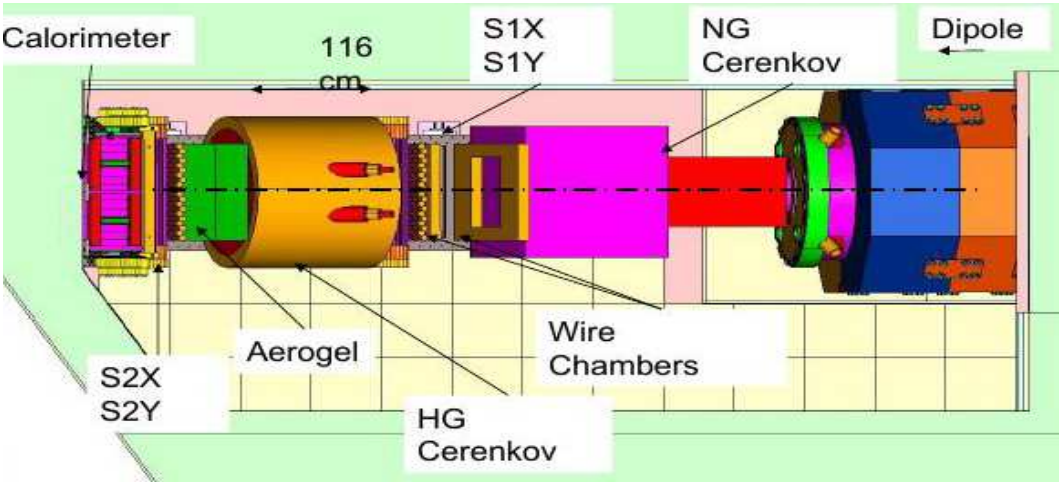

Figure 3.2: View of the detector and triggering inside the shield house

which fall below the threshold velocity of $1/n$ where n is the refraction index of the quartz bar at a given wavelength. The average index of refraction within the quartz bars in the UV is about 1.46. This yields a Cherenkov threshold $\beta_{th} \approx 0.68$ which gives a Cherenkov angle, $\theta_C \approx 43.23$. If total internal reflection is used and a coincidence between top and bottom PMTs is required, the threshold can be raised to $\beta_{th} \approx 0.923$.

By removing the background noise, the hodoscope can provide precise triggering for the desired particles, and efficiently track the location of the particle's interaction on the bars.

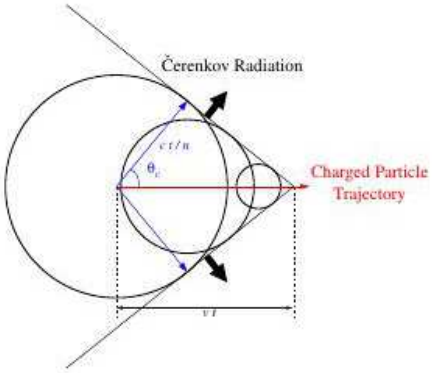

Figure 3.3: Production of Cherenkov radiation for a given particle, [6]

CHAPTER 4

The Quartz Hodoscope

The quartz hodoscope consists of 21 quartz bars. Each bar measures 125 cm long, 5.5 cm wide and 2.5 cm thick. Manufactured by Advanced Glass Industries of Rochester NY, the fused silica (SiO_2) quartz bars (Corning 7980 Grade 0-F) have an excellent UV light transmission, an optical uniformity of 200 mm flatness and an optical grade polish of 25 $\mathring{A}$ rms: These properties give the quartz bars the favorable properties for the SHMS hodoscope as seen in Figure 4.1.

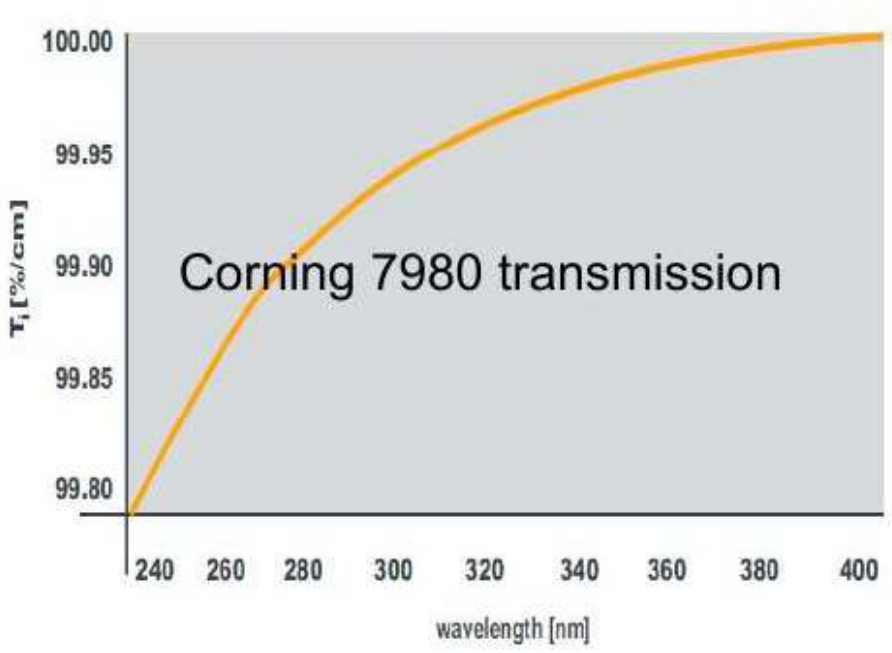

Figure 4.1: Corning 7980 Transmission

Prototyping at NCAT began in 2011, and assembly of the materials and equipment starting in 2012. The assembly of the hodoscope consist of a multi-phased process; testing of the PMTs, preparing the bars and final assembly of PMTs with the quartz.

4.1 Testing of PMTs

Two different PMTs are in use for this project; Photonis XP2020Q and Electronic Tubes (ET) 9814QB. These PMTs where selected because they provide spectral coverage in the UV. This helps increase the amplitude of the collected signals.

Both PMTs are a 12-stage, 51mm round tube with the window material is fused silica with an angle of refraction around 1.48 with the photocathode of Bi-alkali. The Photonis XP2020Q has a spectral range of 150 – 650 nm with maximum sensitivity at 420nm. The ET 9814QB spectral range is 160 – 630 nm with a spectral peaks at 200 & 360 nm.

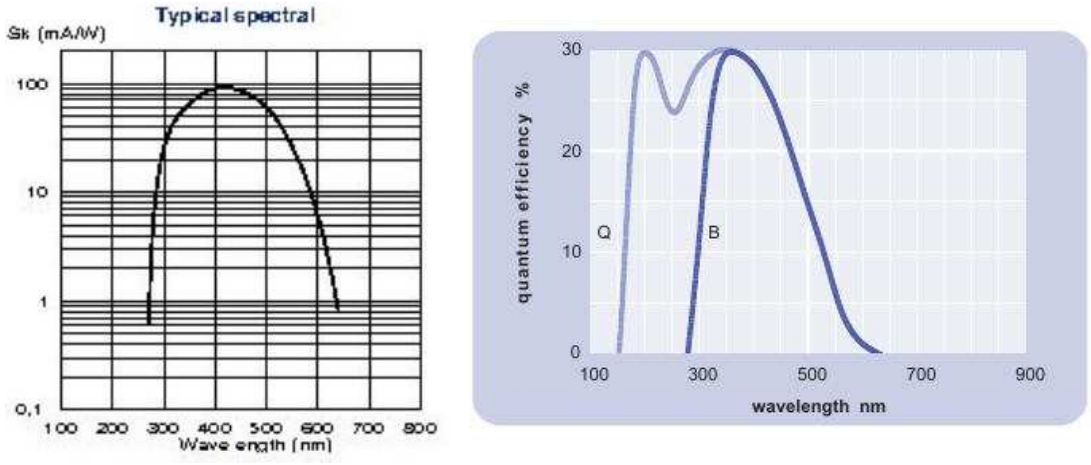

Figure 4.2: Photonis XP2020Q [4] (Left) and ET 9810QB [5] (Right) spectrum from manufacture's data sheet

The tubes are taped with a single layer of electrical tape in order to avoid light leaks and for electrical isolation. The PMTs have a magnetic μ-metal shielding cylinder placed around the tube in order to shield the tube against the Earth's and the spectrometer's magnetic fields. The PMTs are operated at positive HV polarity because of the metallic nature of the surrounding attachment mechanism.

4.2 Visual Inspection of Quartz Bars

During the Summer of 2011, NCAT students cleaned and examined the quartz bar's quality. The testing consisted of shinning a low powered laser light to see any imperfection in the reflective quality of the quartz bar. Once the bar's quality was assured, they were placed back into storage to await assembly.

4.3 Detector Assembly

The overall assembly of the PMT/quartz will consist of different stages; the preparation of the bars, assembly of the brace/bar interface and the actual optical coupling of the PMTs to the bars.

4.3.1 Preparing for Assembly

In preparations for assembly, the bars undergo a detailed process in which they are cleaned, wrapped and taped. Each step was conducted at NCAT by various graduate and undergraduate students. Normally at least two people are needed for the wrapping and tapping steps. List of materials used: 100% Acetone, rubbing alcohol, non-lint towels, Kimwipes, black tedlar, dust free latex gloves, electrical vinyl tape, and black scotch tape.

Cleaning

The cleaning of the raw exposed bars has two main phases. The first is the removal of any residue glue or oils from manufacturing and shipping to NCAT. This is done with an acetone solvent and the non-lint towels until all trace of residues are removed. From here, rubbing alcohol is used to clean the residue of acetone from the bars. All edges are cleaned and visually inspected to ensure clarity.

Wrapping

A single sheet of tedlar paper ($\approx 47\mu$m thick) is cut for each bar. Each sheet is slightly longer than 125cm (the length of the bar) and 32cm wide (two complete wraps around the bar). The bar is laid down on the tedlar so that the long edge of the paper is approximately down the center of one of the 5cm wide surfaces of the bar. While holding down the end of the tedlar to the bar, rotate the bar around so the paper is firm against the bar. No tape or other adhesives are needed to hold the tedlar to the bar if the wrapping is tight around the bar. The paper will be kept tight to the bar and will lay smoothly against the bar once the bar has two complete layers of tedlar.

Taping

Using the black scotch tape$^{(4.3.1)}$, a single strip of tape is applied down the length of the bar along the edge of the tedlar paper. The method deployed during construction was to have one person hold the edge of the tedlar while the other applied the tape. While applying the tape, care must be taken to maintain the tautness of both the tedlar and a straight, smooth fit of the tape against the tedlar. The goal is to have no air bubbles or creases in the tape.

Once the first strip of tape as been applied, flip the bar over and apply another strip of tape to the other wide side of the bar. Then, turn the bar on its side and apply another strip of tape to the narrow side of the bar. Again flip the bar and complete the taping by applying the final strip of tape. The completed bar will have the entire surface of the bar (excluding the end pieces) covered in tape with no air bubbles and no creases. Care must be taken to ensure that the edges of the tape are flush with the rest of the tape so during transport and mounting the tape does not roll up. The two end pieces need to be trimmed of access tedlar and tape so that the ends of the covering match exactly with the bar. Another check of the ends of the bars is needed to ensure the cleanliness of the quartz.

4.3.2 Quartz Bar–PMT Interfacing

Quartz Bar-Brace

The quartz bar to brace interface, Figure 4.3, is constructed of aluminum and has two main pieces; the anchor and flange. The anchor fits directly on the covered quartz bar and is secured in place by an adjustable clamp. The style of clamped used during assembly is an aluminum hose clamp which is tighten using a worm drive screwing mechanism. Care must be taken with the worm drive not to over tighten the screw so the drive does not skip tracks and wear down the groves. The design prints state not to tighten beyond 25 foot/pound, but 20 foot/pounds was enough to secure the brace in place to anchor the PMT.

Figure 4.3: Quartz bar-PMT connector brace

The second piece of the brace is the flange, which is formed to fit around the PMT and connects to the anchor via 6 threaded screws. The inside of the flange was spray painted black to reduce any stray light reflections and subsequently light leaks.

Optical Coupling - Silicone Gel

The silicone gel, RTV615A Potting and Encapsulating Compound, is a commercial product from Momentive. This product was chosen due to the index of refraction, $n \approx 1.41$ [2], which is very close to the index of refraction of the quartz bars, $n \approx 1.46$ in the UV wavelengths, and for its excellent transparency

at UV wavelengths. Figure 4.4 shows the transparency of the gel at thicknesses of 0.25, 0.50, 0.90, and 1.00 mm.

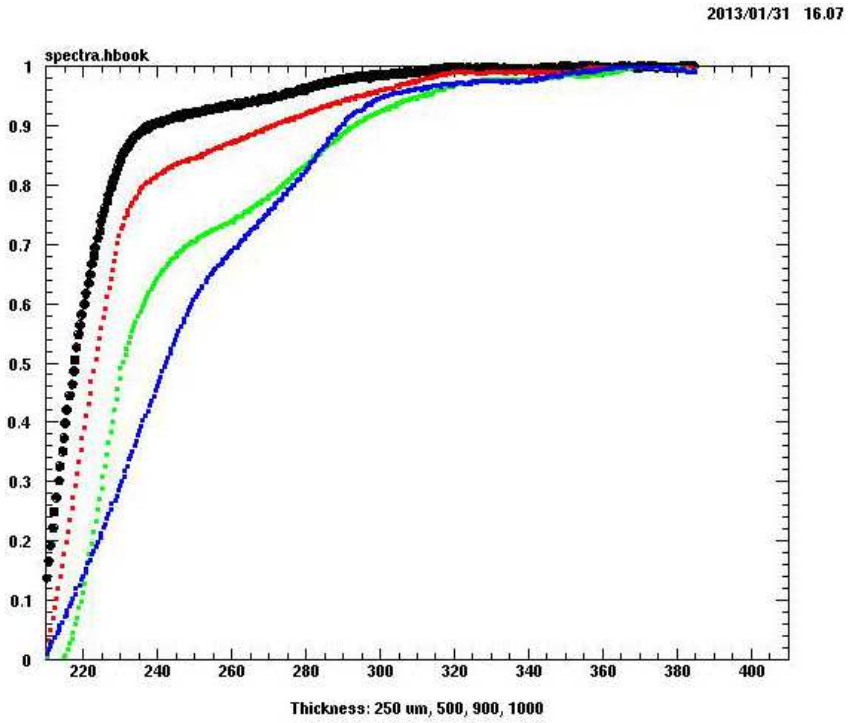

Figure 4.4: Plot of RTV615A thicknesses and transparency

The compound consists of two agents; silicone rubber compound and a curing agent, mixed in at 10:1 ratio. The amount of gel for each bar/PMT interface is determined by the volume of disk with the diameter of the PMT (51mm) and the thickness of the "cookie," 0.9 mm. After the total amount of the compound and curing agent are mixed completely, the compound is placed inside a centrifuge and set to spin for about 15 minutes. This is done to force the air bubbles out of the mixture to ensure a uniform consistency in the gel once it is poured. At room temperature, the specifications indicate that the working time is about 4 hours, sufficient cure time of 24 hours, and complete cure in 7 days. For this interface, a time of $4 - 5$ hours solidifies the compound enough that it will still adhere to the end of bar without leaking down the bar.

4.3.3 Bar – PMT Coupling

The bars are placed vertically in the transportation box with the exposed end completely vertical and level. The PMT with the semi-dry gel is then placed, gel side towards the bar. Ultimately the bar and PMT should stay in this configuration for at least a few hours before securing the PMT with the three threaded rods and the back bracket.

Figure 4.5: View after the three threaded rods have been tightened the back brace securing the PMT to the quartz bar

Using the three rods, secure the PMT so that it is level and tight to the bar. The design instructions state to tighten the nuts down until the lock washer is flat and secure against the back bracket and the nut. Once all the PMTs are secured the entire rack is turned upside down and the other end has PMTs applied to it in the same fashion.

4.4 Transportation

For storage and transportation purposes, four wooden crates were constructed. Each crate has a rack which fits five quartz bars. The bars are secured in place by a bolt and wing nut configuration which lock down the quartz bars inside the rack. The cover of the crate is then screwed in place and is designed to hold the racks in place during transport.

Figure 4.6: All 4 wooden crates and racks filled with quartz bars waiting transport to JLab

A rack can be easily removed from its crate and is used in the testing and calibration phase. Figure 5.1 shows a rack in place during testing.

CHAPTER 5
Calibration with Cosmic Rays

5.1 Set up

As described in 4.4, the bars are placed in the wooden carrying 'racks' and identified numerically by the rack in which they are placed. The bars are identified numerically by, 1 – 21, starting from the first rack. The PMTs are likewise numbered from 1 – 42 with PMTs 1 and 2 attached to bar 1, PMTs 3 and 4 to bar 2 . . . and so on. The only exception is when a bar was found to have unusual data which need to be reexamined or the bar was on top or bottom of the rack and a second collection of data was taken to ensure the accuracy of the results.

Each rack is tested individually using cosmic muon rays. The rack is placed so that the bars are stacked vertically as shown in Figure 5.1. Two scintillators are deployed for position referencing and as part of the overall triggering of data collection. One scintillator is placed above the rack, and one below the rack. Three positions are used in the calibration; the middle of the bars ≈ 62 cm from each end of the bar, and at each quarter point of the bars ≈ 30 cm from each end of the bar.

5.2 Data

The data for calibration is organized by the position the data are collected, the rack, bar and PMT for each data set.

Figure 5.1: Setup for cosmic ray testing

5.2.1 Data Collection

Timing and amplitude information is collected from PMT signals. Figure 5.2 is an outline of the electronics diagram. Signals from the PMTs are sent through the electronics and once all the proper logic has been fulfilled, a 250 ns gate is opened in the timing to digital conversion(TDC) and analog to digital conversion (ADC) modules which are read by the CAMAC controler.

5.2.2 Data Analysis Code

The current analysis technique utilizes standard FORTRAN commands and PAW++ [3] calls. The existing code works and produces positive results, but can be cumbersome at times, and some of the analysis still has be to done by visual trial and error methods. A new analysis was developed in a computer algebra system, Mathematica^{TM}, which handles the data set with minimal changes to the code and removes the need to change programs during analysis.

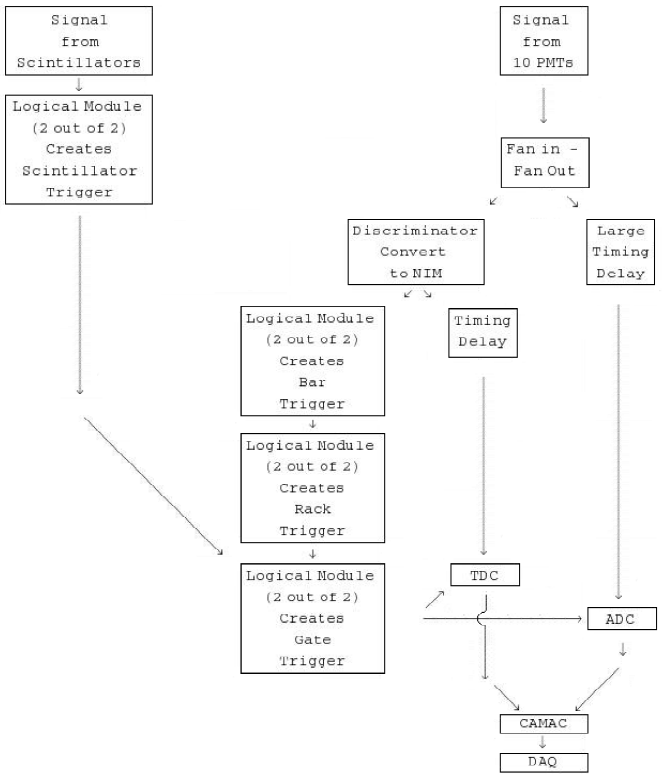

Figure 5.2: Electronics flow chart

FORTRAN/PAW++

The FORTRAN code is currently used, and has been for years with positive results. The code needs to be calibrated for each set of data, before clear results can be obtained. This calibration comes from an analysis of the data at different positions of the top and bottom scintillators. This requires an edit of the code when either the position changes and/or new data set is introduced. The code is then required to be recompiled and then executed before PAW++ is used to view the results of the analysis. Within PAW++, histogram fitting command and other functions are used to visually examine ADC histograms to generate data which then needs to be calculated to produce the number of photo-electrons produced. This takes time and can be a bit arbitrary when determining the precise range of the data that is needed to be fitted.

Mathematica

The procedure now developed takes in the data file, reads and sorts the data by the PMT numbers and separates the TDC from the ADC data which can then be used by Mathematica. From here, procedures and newly developed functions are called to analyze the data. All the analysis is done internally and produces the number of photo-electrons, efficiency of the bars, raw histograms of the ADC and TDC data, position resolution plots of the events on the bar.

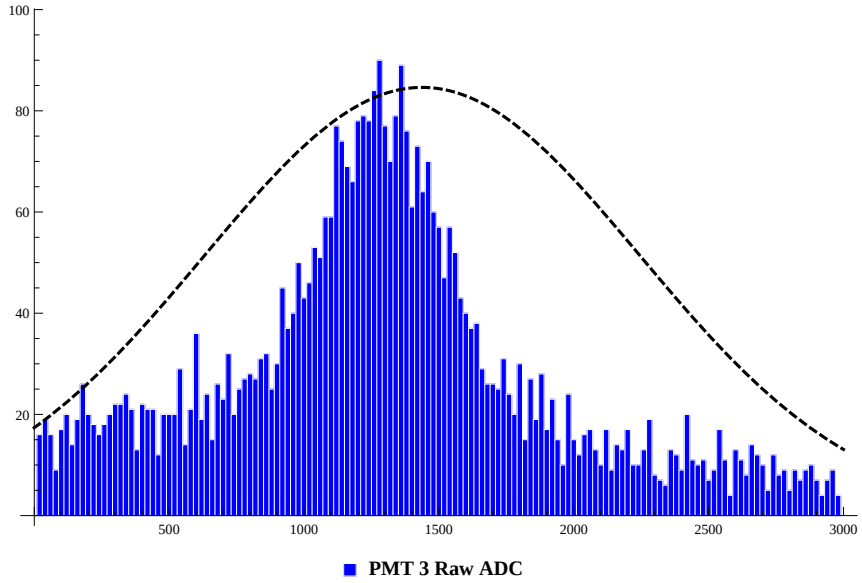

PMT#	Peak	Init Mean	Init STD
3	1280	1438	808

Figure 5.3: Gaussian curve fit to all data, PMT 3, rack 04

Part of the automation of the data analysis is fitting curves to the data without the user conducting trial and error. The peaks of the ADC histograms tend to be well defined and can be fitted with a Gaussian curve. Attempting to do so from the entire set of data proved to be dissatisfying, as Figure 5.3 shows.

The solution is to use the statistics from the data set and chop off as much of the data that is not around the peak as possible. Using the peak value, one standard deviation is added and subtracted to define the new range for the statistics. The peak value is found by counting the total number of values in each bin

and retrieving the largest value. The standard deviation is found from in internal call within Mathematica.

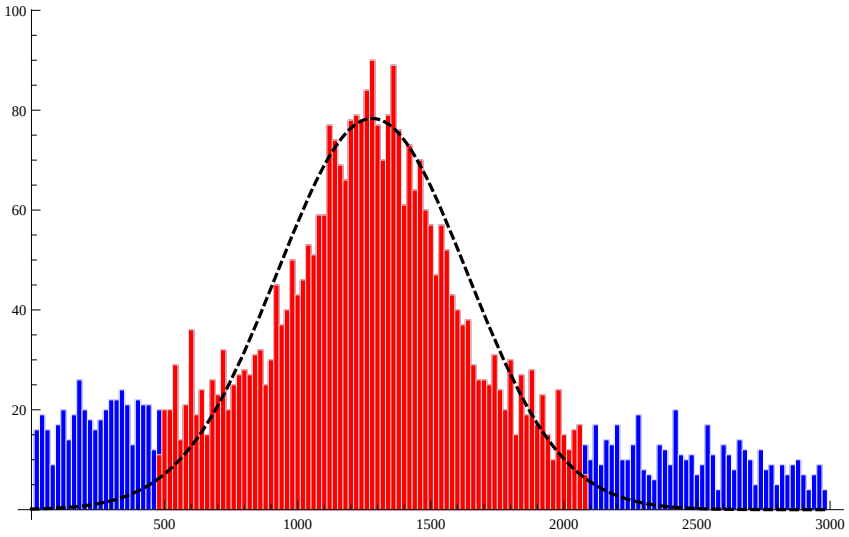

PMT#	Peak	Init Mean	Mean 1	Init STD	STD 1	#PE 1
3	1280	1438	1329	808	351	14

Figure 5.4: Gaussian curve fit to a reduced range from the data, PMT 3, rack 04

Again, as seen from Figure 5.4, the curve has not been properly fitted so another reduction of the data set is taken using the same method as before, now with a smaller standard deviation around the peak.

The final reduction of the data yields a Gaussian curve which fits the data, Figure 5.5.

5.3 Analyzed Data

5.3.1 Rack 01

Muon Track Close to Even PMT

Set 20 `(07-23-2013_set20)` has the muon track close ($\approx 31cm$) to the Even numbered PMTs. Tables 5.1 and 5.2 shows an example of some of that data collected at this position for this data set.

10501 events were collected and the following, Table 5.3, shows the breakdown of which PMT was

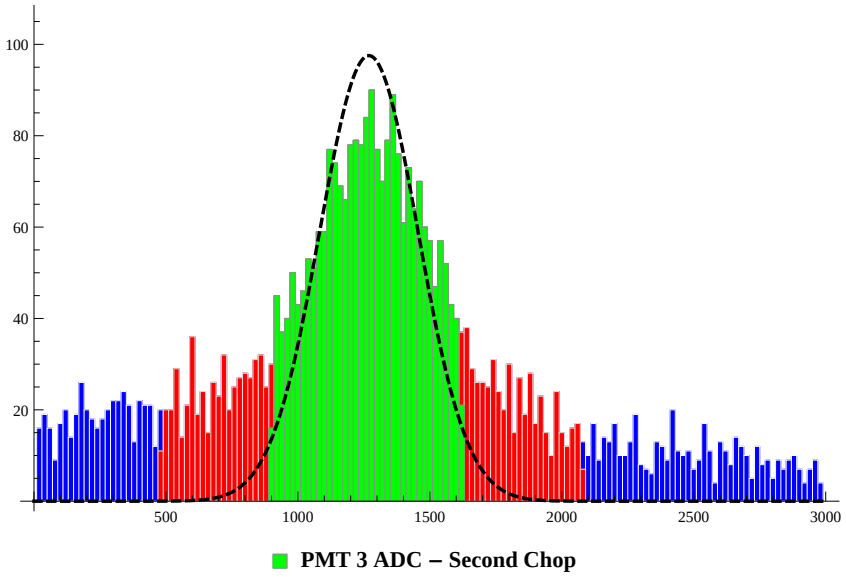

PMT#	Peak	Init Mean	Mean 1	Mean 2	Init STD	STD 1	STD 2
3	1280	1438	1329	1309	808	351	180

Figure 5.5: Gaussian curve fit to a reduced range from the data, PMT 3, rack 04

tested, the high voltage used during the testing, the mean ADC value and standard deviation for each PMT, along with the position resolution for each bar. As shown in the ADC histograms, PMT numbers 5, 6, & 10 did not yield usable ADC values (this is true for all three measurements). These PMTs are re-gelled and tested again.

Muon Track Close to Middle of Bar

Set 21 `(07-31-2013_set21)` has the muon track ($\approx 62cm$) from each end of the bar.

10256 events were collected and the following, Table 5.4, shows the breakdown of which PMT was tested, the high voltage used during the testing, the mean ADC value and standard deviation for each PMT, along with the position resolution for each bar. As shown in the ADC histograms, PMT numbers 5, 6, & 10 did not yield usable ADC values (this is true for all three measurements). These PMTs are re-gelled and tested again.

Muon Track Close to Odd PMT

Set 22 (`08-09-2013_set22`) has the muon track close ($\approx 31cm$) to the odd numbered PMTs.

15961 events were collected and the following, Table 5.5, shows the breakdown of which PMT was tested, the high voltage used during the testing, the mean ADC value and standard deviation for each PMT, along with the position resolution for each bar. As shown in the ADC histograms, PMT numbers 5, 6, & 10 did not yield usable ADC values (this is true for all three measurements). These PMTs are re-gelled and tested again.

Table 5.1: Sample of TDC data from data set 20

TDC01	TDC02	TDC03	TDC04	TDC05	TDC06	TDC07	TDC08	TDC09	TDC10
677	240	342	377	504	589	534	618	461	746
647	237	351	379	531	595	518	619	417	762
749	231	419	374	516	588	628	617	493	745
560	257	207	380	463	599	577	621	450	778
631	243	326	388	510	600	496	632	393	766
653	242	340	387	597	588	531	621	424	766
558	148	252	304	440	1264	430	528	335	1122
665	241	329	379	568	587	4083	4083	433	762
632	240	325	380	491	593	533	620	423	753
635	254	340	393	619	605	511	640	416	801
673	240	359	379	511	599	555	617	414	758

Table 5.2: Sample of ADC data from data set 20

ADC01	ADC02	ADC03	ADC04	ADC05	ADC06	ADC07	ADC08	ADC09	ADC10
311	1323	1086	1657	382	1298	455	1214	560	671
1347	1798	1369	1237	440	932	910	1028	1347	736
391	1484	341	1626	254	958	164	1204	232	646
1675	4095	1389	3883	102	1540	442	2493	1298	1042
1210	785	1966	1293	661	773	1130	962	2543	573
610	1441	1169	1274	588	1980	1597	2037	1864	840
953	444	1145	417	368	177	540	485	311	195
1332	2686	947	1323	101	644	0	0	1785	1047
772	1019	2584	1739	368	915	1055	1193	935	857
679	1636	1073	1354	508	1286	490	1147	1045	354
182	1253	902	1421	523	1128	92	1161	1191	955

Table 5.3: Rack 01, Close to Even PMT

PMT #	High Voltage (kV)	$\bar{x}$	σ	Position resolution (cm)
1	19	802	155	Bar 01
2	20	1304	160	2.60
3	20	1310	165	Bar 02
4	20	1349	157	2.45
5	20	318	112	Bar 03
6	20	573	152	2.83
7	20	812	154	Bar 04
8	20	1077	142	2.00
9	20	993	155	Bar 05
10	20	444	132	2.60

Table 5.4: Rack 01, Close to middle of bar

PMT #	High Voltage (kV)	$\bar{x}$	σ	Position resolution (cm)
1	1.9	869	151	Bar 01
2	2.0	1170	157	1.59
3	2.0	1398	164	Bar 02
4	2.0	1242	150	1.56
5	2.0	302	106	Bar 03
6	2.0	602	158	1.71
7	2.0	948	139	Bar 04
8	2.0	966	133	1.67
9	2.0	1064	151	Bar 05
10	2.0	418	120	1.60

Table 5.5: Rack 01, Close to odd PMTs

PMT #	High Voltage (kV)	$\bar{x}$	σ	Position resolution (cm)
1	1.9	976	147	Bar 01
2	2.0	1011	160	2.21
3	2.0	1517	161	Bar 02
4	2.0	1093	150	2.22
5	2.0	311	111	Bar 03
6	2.0	559	152	2.49
7	2.0	1100	140	Bar 04
8	2.0	853	130	2.32
9	2.0	1227	156	Bar 05
10	2.0	349	103	2.20

5.3.2 Rack 02

Muon Track Close to Even PMT

Set 23 (`09-12-2013_set23`) has the muon track close ($\approx 31cm$) to the even numbered PMTs.

9931 events were collected and the following, Table 5.6, shows the breakdown of which PMT was tested, the high voltage used during the testing, the mean ADC value and standard deviation for each PMT, along with the position resolution for each bar.

Muon Track Close to Middle

Set 24 `(09-26-2013_set24)` has the muon track close ($\approx 62cm$) to the even numbered PMTs.

9984 events were collected and the following, Table 5.7, shows the breakdown of which PMT was tested, the high voltage used during the testing, the mean ADC value and standard deviation for each PMT, along with the position resolution for each bar.

Muon Track Close to Odd PMT

Set 25 `(10-07-2013_set25)` has the muon track close ($\approx 31cm$) to the odd numbered PMTs.

10099 events were collected and the following, Table 5.8, shows the breakdown of which PMT was tested, the high voltage used during the testing, the mean ADC value and standard deviation for each PMT, along with the position resolution for each bar.

Table 5.6: Rack 02, Close to even PMTs

PMT #	High Voltage (kV)	$\bar{x}$	σ	Position resolution (cm)
11	1.8	1327	151	Bar 06
12	1.8	867	142	1.92
13	1.8	1055	130	Bar 07
14	1.8	1085	164	1.95
15	1.8	820	132	Bar 08
16	1.8	556	126	1.93
17	1.8	1042	142	Bar 09
18	1.8	719	133	1.97
19	1.8	895	143	Bar 10
20	1.8	935	184	1.90

Table 5.7: Rack 02, Close to middle of bar

PMT #	High Voltage (kV)	$\bar{x}$	σ	Position resolution (cm)
11	1.8	1172	150	Bar 06
12	1.8	1006	150	1.53
13	1.8	928	139	Bar 07
14	1.8	1309	163	1.55
15	1.8	693	134	Bar 08
16	1.8	680	136	1.53
17	1.8	908	148	Bar 09
18	1.8	840	140	1.58
19	1.8	773	145	Bar 10
20	1.8	1096	193	1.55

Table 5.8: Rack 02, Close to odd PMTs

PMT #	High Voltage (kV)	$\bar{x}$	σ	Position resolution (cm)
11	1.8	1027	158	Bar 06
12	1.8	1122	155	1.86
13	1.8	810	144	Bar 07
14	1.8	1522	177	1.83
15	1.8	589	135	Bar 08
16	1.8	840	143	1.84
17	1.8	774	159	Bar 09
18	1.8	941	154	1.86
19	1.8	643	155	Bar 10
20	1.8	1260	201	1.85

5.3.3 Rack 03

Due to the high position resolution from the previous racks, only data collected for rack 03 is from the middle position to test gel viability and hardware reliability.

Muon Track Close to Middle

Set 39 `(4-01-2014_set39)` has the muon track close ($\approx 62cm$) to the even numbered PMTs.

10070 events were collected and the following, Table 5.9, shows the breakdown of which PMT was tested, the high voltage used during the testing, the mean ADC value and standard deviation for each PMT, along with the position resolution for each bar.

Table 5.9: Rack 03, Close to middle of bar

PMT #	High Voltage (kV)	$\bar{x}$	σ	Position resolution (cm)
21	2.1	714	199	Bar 11
22	2.0	1384	178	2.19
23	2.1	743	206	Bar 12
24	1.8	789	183	2.17
25	2.1	725	191	Bar 13
26	2.2	742	193	2.25
27	2.0	995	179	Bar 14
28	2.0	934	216	2.17
29	2.1	647	180	Bar 15
30	2.2	663	180	2.20

5.4 Observations Made from Data Analysis

5.4.1 Position Resolution

To find the position resolution, each event was analysed. First the null TDC event values are removed; every value lower than 10 and every value above 4000. Next each odd numbered PMT TDC value is subtracted from the corresponding even number PMT TDC value. The result is then multiplied by the speed of light inside the quartz bar, given by the sine of the Cherenkov angle multiplied by the ratio of the speed of light in a vacuum and the refraction index of the quartz bar, which comes out to be ≈ 0.13 cm/ps.

Table 5.10: Average position resolution by Muon track position on the bar

Muon Track Position	Position Resolution (cm)	Standard Deviation
≈ 30 cm from Even PMTs	2.22	0.37
Close to Middle of Bar	1.79	0.30
≈ 30 cm from Odd PMTs	2.07	0.25

As seen in Table 5.10, the average position resolution of the detectors at the given positions is consistent given the size of the top and bottom scintillators, 10 cm wide.

5.4.2 Multiple TDC Peaks

Some clear trends are observed from the data. In a few cases the TDC data shows more than a single TDC peak as seen in Figure 5.6. These multiple peaks turn out to be imperfections in the quartz-PMT interface gel. This is confirmed by a removal of the PMT from the bar in an inspection of interface. The silicon gel appears to have not adhered to the quartz bar. This in turn led to an air pocket forming and creating a reflection of light within the interface. To remedy the problem, the PMT and the end of the quartz bar are cleaned and the PMT is reattached to the quartz bar with new silicon gel. The results, as shown in Figure 5.7, the re-gelling eliminated the multiple peaks in the TDC data.

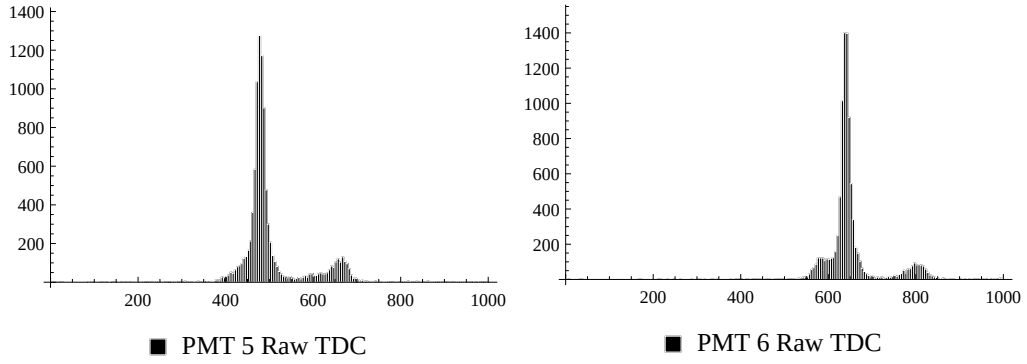

Figure 5.6: 2 peaks in TDC data indicated a possible impurities in the quartz-PMT interface, PMT 5 & 6, rack 01

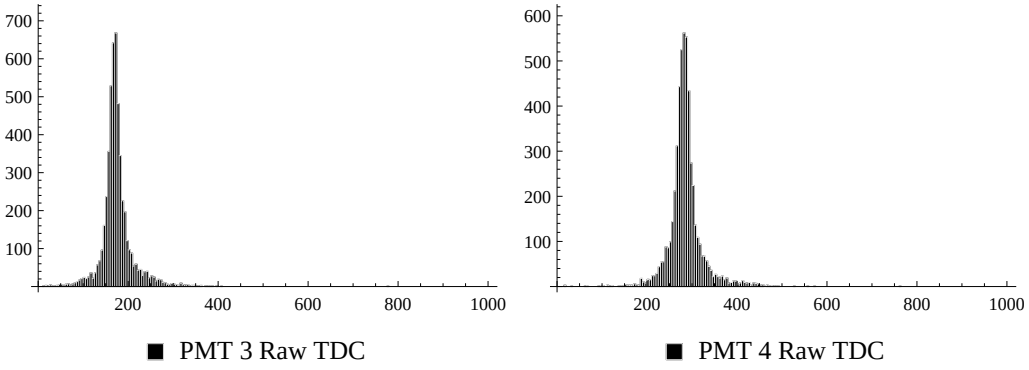

Figure 5.7: Results of re-gelling the PMTs, PMT 5 & 6, rack 01

CHAPTER 6

Conclusion

A 21 quartz bar hodoscope has been constructed at NCAT. A detailed description of the procedure of the assembly of the hodoscope is provided. The materials which are used along with solutions to the issues which were encountered during the assembly have been presented. Another method of data analysis has been developed and can be used in finding any further issues with the rest of the detector assembly.

A sophiscicated way of coupling PMTs to the quartz bars has been successfully implemented. Issues with light reflection has been identifed and solved. Position resolution of the detector shows that a beam focused on the central portion of the detector can be tracked within 2.0 cm of the actual location on the quartz bars. Future work is still needed, and currently on going, includes more collection of data at different positions along the racks.

REFERENCES

[1] Hall_C 12 GeV Approved Experiments. Retrieved June 26, 2014, from http://www.jlab.org/exp_prog/generated/12GeV/apphallc.html.

[2] Momentive RTV615 Technical Data Sheet. Retrieved June 20,2014, from http://www.momentive.com.

[3] Physics Analysis Workstation (PAW++). Retrieved June 20,2014, from http://paw.web.cern.ch/paw/.

[4] Photomultiplier XP2020Q, 2007. Manufacture's data sheet.

[5] ET Enterprises 9818B series data sheet, 2012. Manufacture's data sheet.

[6] Wenliang Li. Heavy Gas Cherenkov Detector Construction for Hall C at Thomas Jefferson National Accelerator Facility. Master's thesis, University of Regina, 2012.